Journal of Alloys and Compounds 509 (2011) 5537–5544

Contents lists available at ScienceDirect

Journal of Alloys and Compounds

journal homepage: www.elsevier.com/locate/jallcom

Magnetic and electrical transport properties of $La_{0.5}A_{0.5}CoO_3$ nanoparticles (A = Sr, Ca, and Ba)

B. Roy [a], S. Das [b,*]

[a] Department of Physics, Ramakrishna Mission Vidyamandira, Belur Math, Howrah 711202, India
[b] ECMP Division, Saha Institute of Nuclear Physics, 1/AF Bidhannagar, Kolkata 700064, India

ARTICLE INFO

Article history:
Received 27 July 2010
Received in revised form 8 January 2011
Accepted 19 January 2011
Available online 21 March 2011

Keywords:
Nanostructured materials
Sol–gel process
Electrical transport
Magnetization
TEM
X-ray diffraction

ABSTRACT

We have investigated the effect of particle size on the electrical transport and magnetic properties of $La_{0.5}A_{0.5}CoO_3$ (A = Sr, Ca, and Ba) nanoparticles synthesized by sol–gel technique. A size-induced metal to insulator transition is observed in the resistivity behaviour of Sr- and Ba-doped samples as the dimension changes from higher to lower ones. The magnetoresistance exhibits almost linear behaviour throughout the studied field range. The zero-field-cooled (ZFC) and field-cooled (FC) magnetizations display a broad paramagnetic to ferromagnetic transition at T_C with a large magnetic irreversibility. The magnetization results indicate that Co^{3+} ions are in the intermediate spin state but Co^{4+} ions stay in a mixture of intermediate and high spin states. The observed frequency dependent shoulder in the in-phase and the peak in the out of phase component of the *ac* susceptibility indicate the glassy nature of the samples. The analysis of the *ac* magnetization results suggests that the magnetic behaviour is consistent with the cluster glass model.

1. Introduction

Recently temperature-induced electronic and spin state transition in undoped and doped $LaCoO_3$ has attracted much attention. The additional spin state degree of freedom gives rise to new physical properties, leading to unusual magnetic and transport properties. The ground state of $LaCoO_3$ with Co^{3+} ($3d^6$) ions is a charge transfer type insulator with no magnetic order. The magnetic susceptibility increases exponentially with increasing temperature to reach a maximum near 100 K. This transition was initially explained as a spin state transition from a low spin non-magnetic state (t_{2g}^6, $S = 0$, LS) to a high spin state ($t_{2g}^4 e_g^2$, $S = 2$, HS) [1–4] but later the existence of an intermediate spin state ($t_{2g}^5 e_g^1$, $S = 1$, IS) was proposed. The spin state transition originates from a competition between crystal field splitting energy and interatomic Hund exchange coupling energy. The results of local density approximation (LDA + U) [5] reveal that strong hybridization between ligand O 2p and Co 3d orbitals stabilizes the intermediate spin state with introduction of holes in the oxygen 2p orbital instead of the high spin state. Due to very small energy difference between the spin states, the variation of temperature drives a gradual switch over from low spin to intermediate spin or high spin states for Co ions. The substitution of trivalent La^{3+} by divalent alkaline earth metals (A) such as Ca^{2+}, Sr^{2+} or Ba^{2+}, converts Co^{3+} to Co^{4+} and the magnetic properties of cobaltites depend on the spin states of Co^{3+} and Co^{4+} ions. In $La_{1-x}A_xCoO_3$, Co ions can have six different spin states (low, intermediate and high) for Co^{3+} and Co^{4+} among which a transition takes place by a change of external stimuli like temperature and pressure. Ferromagnetic (FM) ordering appears due to the double exchange interactions between Co^{3+} and Co^{4+} ions. Moreover, the antiferromagnetic (AFM) interaction is also enhanced by Co^{4+}–Co^{4+} superexchange couplings in addition to the pre-existing Co^{3+}–Co^{3+} interaction. Most of the studies on cobaltites deals with $La_{1-x}Sr_xCoO_3$. Compared to Sr-doped cobaltite, Ba- and Ca-doped cobaltites [6–11] did not receive much attention. Research on nanocrystalline materials has attracted much attention due to their interesting properties. A large fraction of the atoms in the nanoparticles are surface atoms which influence the magnetic properties significantly. The magnetization strongly depends on the particle size, core/shell morphology, temperature, surface/interface effect, magnetic interactions, etc. We have prepared $La_{0.5}A_{0.5}CoO_3$ (A = Sr, Ca, and Ba) nanoparticles by sol–gel process and presented the results of structure, electrical transport and magnetic properties of these samples to elucidate the modification of their electronic and magnetic properties due to the nano-size of the particles.

2. Experimental

$La_{0.5}Sr_{0.5}CoO_3$, $La_{0.5}Ca_{0.5}CoO_3$ and $La_{0.5}Ba_{0.5}CoO_3$ were prepared from stoichiometric highly pure La_2O_3, $CaCO_3$, $SrCO_3$, $BaCO_3$ and $Co(NO_3)_2{\cdot}6H_2O$ (*Alfa-Aesar*) by

* Corresponding author.
E-mail address: sailendranath.das@saha.ac.in (S. Das).

0925-8388/$ – see front matter © 2011 Elsevier B.V. All rights reserved.
doi:10.1016/j.jallcom.2011.01.135

sol–gel method. Before weighing, La_2O_3 was preheated at 1000 °C for several hours to decompose possible carbonates and hydroxides. La_2O_3, $SrCO_3$, $CaCO_3$, and $BaCO_3$ were converted into their respective soluble nitrates by dissolving them in dilute HNO_3 at room temperature. $Co(NO_3)_2{\cdot}6H_2O$ readily dissolves in deionized water. All the individual nitrates were mixed together with citric acid and deionized water while stirring, to form a homogeneous mixture. The resultant solution was heated at low temperature for several hours to evaporate water and finally gel is formed. The gel was burnt to dried powder and the collected powder was heated at 425 °C for a long time giving a black powder. The precursor was separated into parts and pelletized. Each part was calcined at different temperatures from 650 °C to 1100 °C for 5 h to obtain different particle sizes. The phase purity of the samples was judged by X-ray powder diffraction (Philips PW diffractometer 1820) using Cu K_α radiation and the X-ray diffraction data of the samples were analyzed with Rietveld method using FULLPROF program [12]. The particle size was determined analyzing the broadened X-ray line width using Scherrer's formula. The particle morphology was examined and the sizes were measured by the transmission electron microscope (TEM). Magnetization measurement of the samples was performed with a Superconducting Quantum Interference Device (SQUID, Quantum Design MPMS-XL) in the temperature range 5–300 K and under magnetic fields up to 50 kOe. The temperature dependence of *ac* susceptibility was studied at different frequencies. The resistivity was measured by standard four probes technique whereas the magnetoresistance measurement was made with direct current perpendicular to the magnetic field direction in the temperature range of 4–300 K using an Oxford cryostat equipped with 8 T magnetic field.

3. Results

3.1. X-ray diffraction and transmission electron micrographs

The analysis of the powder X-ray diffraction (XRD) profile confirmed that all samples are in single phase. Fig. 1 displays some typical plots of X-ray diffraction patterns of $La_{0.5}A_{0.5}CoO_3$. The XRD data of $La_{0.5}Sr_{0.5}CoO_3$ and $La_{0.5}Ca_{0.5}CoO_3$ are refined (Fig. 1(a) and (b)), assuming a rhombohedral unit cell containing two formula units with $R\bar{3}C$ space group. The refinement results of the crystal structure for nanoparticle samples are in good agreement with those obtained for bulk samples [13]. It is found from the Rietveld analysis that $La_{0.5}Ba_{0.5}CoO_3$ has a cubic structure and the diffraction patterns can be indexed with space group $Pm3m$ [14]. The structural parameters obtained are in agreement with those reported in the literatures [10,14]. Lattice parameters and refinement parameters are summarized in Table 1. The average size (D) of the particles is calculated using Scherrer's formula given by $D = k\lambda/\beta\cos\theta$, where k is the particle shape factor (=0.89, considering circular shape of the nano particles), λ is the wavelength of Cu K_α radiation (=1.5406 Å), β is the full width at half maximum of the XRD peak and θ is the diffraction angle of the peak. The size of the particle was also confirmed by TEM measurement. The typical transmission electron microscope images of $La_{0.5}A_{0.5}CoO_3$ are shown in Fig. 2. The TEM image unravels that the nanoparticles of the sample studied have nearly sphere-like elementary shape and the particles are arranged in chains of nonagglomerate individual nanoparticles with a cluster-forming tendency.

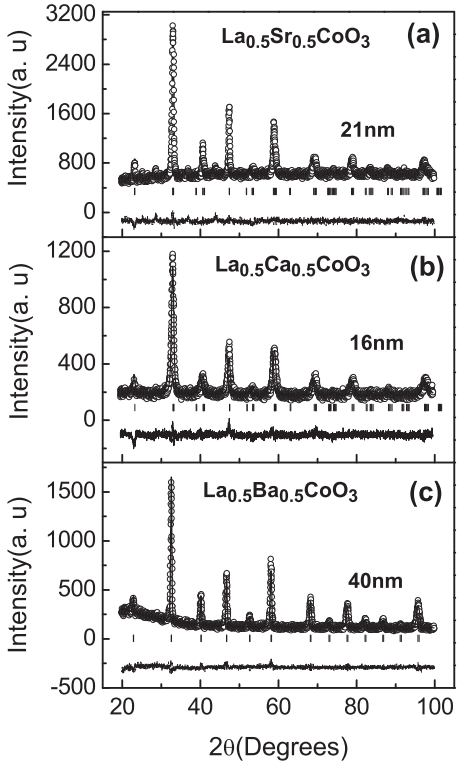

Fig. 1. X-ray powder diffraction patterns with the Rietveld refinement curves for the (a) $La_{0.5}Sr_{0.5}CoO_3$, (b) $La_{0.5}Ca_{0.5}CoO_3$, and (c) $La_{0.5}Ba_{0.5}CoO_3$ samples with dimensions 21 nm, 16 nm, and 40 nm, respectively. The observed intensity are shown by open circle (○) and the solid line is the calculated intensity; the small vertical lines are the position of Bragg reflections and the lower curve is the difference between the observed and the calculated intensities.

3.2. Resistivity

In Fig. 3 we have presented the temperature dependence of the resistivity of $La_{0.5}A_{0.5}CoO_3$ nanoparticles of different sizes under zero field. From the resistivity measurement, it is seen that a size-induced metal to insulator transition takes place in $La_{0.5}Sr_{0.5}CoO_3$ [15] and $La_{0.5}Ba_{0.5}CoO_3$ samples. The resistivity of the semiconducting samples increases with the decrease of particle size implying that the decrease of size relatively increases the insulating regions due to the enhancement of the grain boundary effect and also the disorder on the surface. $\rho(T)$ evolves from strongly insulating for low size ($d\rho/dT < 0$) to weakly insulating (21 nm of Sr-doped, 33 nm of Ca-doped and 40 nm of Ba-doped sample) for higher size and the temperature dependence seems to be monotonous. The Sr-doped 21 nm sample shows a weak

Table 1
Particle size from XRD and TEM, annealing temperature (T_{ann}), lattice parameters, oxygen fractional coordinate (x) and χ^2 for $La_{0.5}Sr_{0.5}CoO_3$, $La_{0.5}Ca_{0.5}CoO_3$ and $La_{0.5}Ba_{0.5}CoO_3$ compounds.

Compounds	Particle size (nm)		T_{ann} (°C)	$a = b$ (Å)	c (Å)	x	χ^2
	XRD	TEM					
$La_{0.5}Sr_{0.5}CoO_3$	18.8	15	650	4.7029	13.1694	0.4628(8)	1.07
	22.5	21	700	4.7133	13.2049	0.4677(2)	1.17
	26.3	25	850	4.7153	13.2496	0.4637(1)	1.22
$La_{0.5}Ca_{0.5}CoO_3$	17.8	16	750	4.6913	13.2031	0.4808(5)	1.38
	26.6	28	875	4.6986	13.2065	0.5147(4)	1.92
	32.1	33	950	4.7008	13.2093	0.5192(7)	1.75
$La_{0.5}Ba_{0.5}CoO_3$	27.6	26	875	3.8624	$c = a$	[a]	1.89
	40.5	40	1000	3.8880	$c = a$	[a]	1.35
	49.8	51	1100	3.8972	$c = a$	[a]	1.67

[a] Crystallographic sites are (1/2, 1/2, 1/2), (0, 0, 0) and (0, 1/2, 0) for La/Ba, Co and O, respectively.

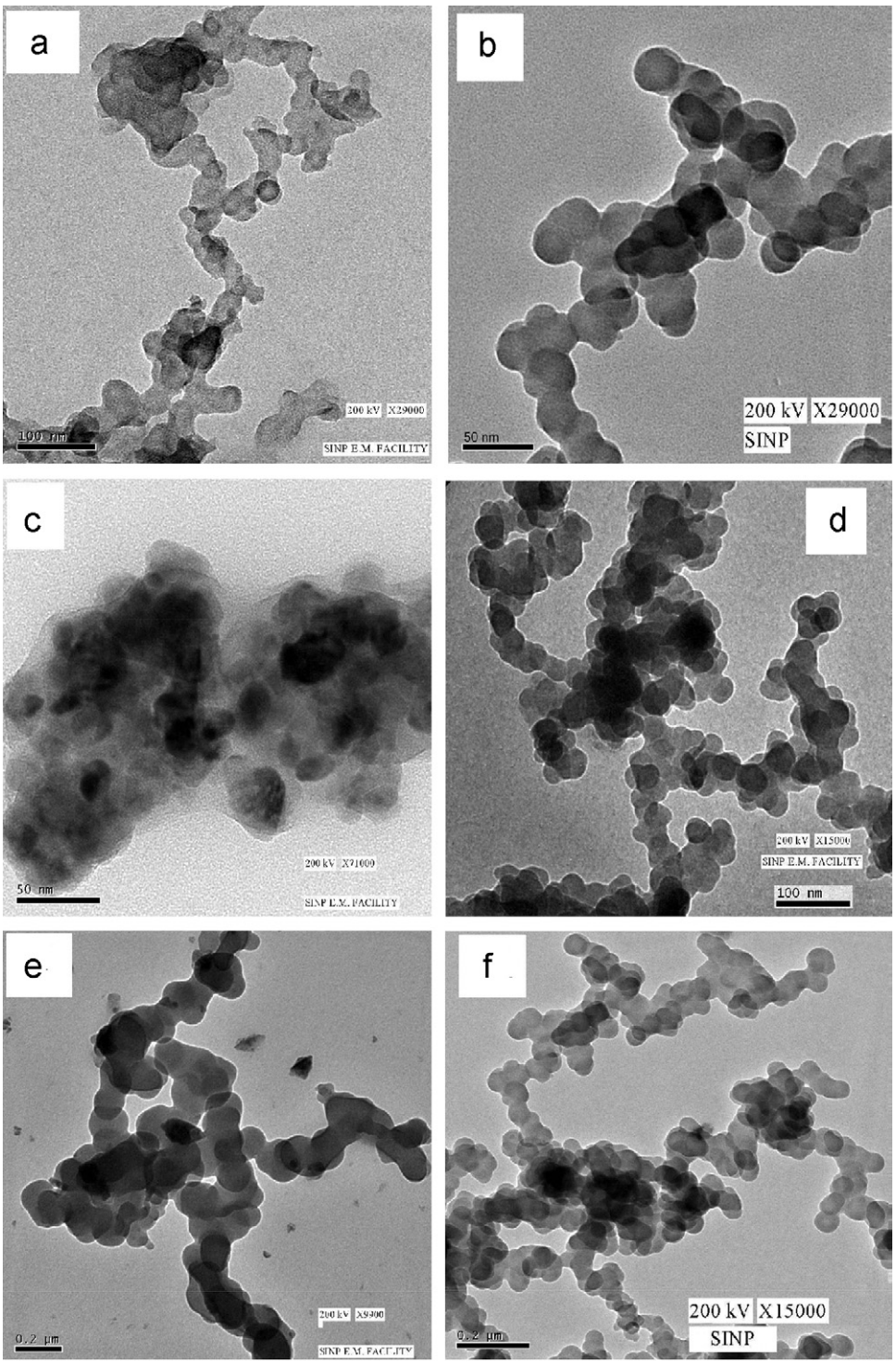

Fig. 2. Transmission electron micrographs of the $La_{0.5}Sr_{0.5}CoO_3$ with dimension of 21 nm (a) and 25 nm (b), $La_{0.5}Ca_{0.5}CoO_3$ sample with 16 nm (c) and 28 nm (d) particle size, and (e) 40 nm and (f) 51 nm samples of $La_{0.5}Ba_{0.5}CoO_3$.

increase of $\rho(T)$ with the decrease in temperature from 300 K down to 210 K and there is a slight decrease of $\rho(T)$ below 210 K. Finally these samples show a low temperature increase of resistivity. Similar behaviour of $\rho(T)$ is observed in 33 nm Ca-doped and 40 nm Ba-doped samples. The samples such as 25 nm $La_{0.5}Sr_{0.5}CoO_3$ and 51 nm $La_{0.5}Ba_{0.5}CoO_3$ exhibit a metallic behaviour with a kink in resistivity at transition temperature, T_C, which may be caused by spin disordering. Above T_C the material shows a semimetallic behaviour with a sudden increase of the electrical conductivity.

3.3. Magnetoresistance

The magnetoresistance (MR) data were collected by cooling the sample to the measurement temperature in zero magnetic field ($H = 0$) then sweeping from $H = 0$ to 70 kOe. Fig. 4(a) and (b) displays the field variation of the magnetoresistance of the 15 nm and 21 nm samples of $La_{0.5}Sr_{0.5}CoO_3$ and Fig. 4(c) represents the field induced magnetoresistance of $La_{0.5}Ca_{0.5}CoO_3$ samples at various temperatures. The magnetoresistance of the samples shows a monotonic

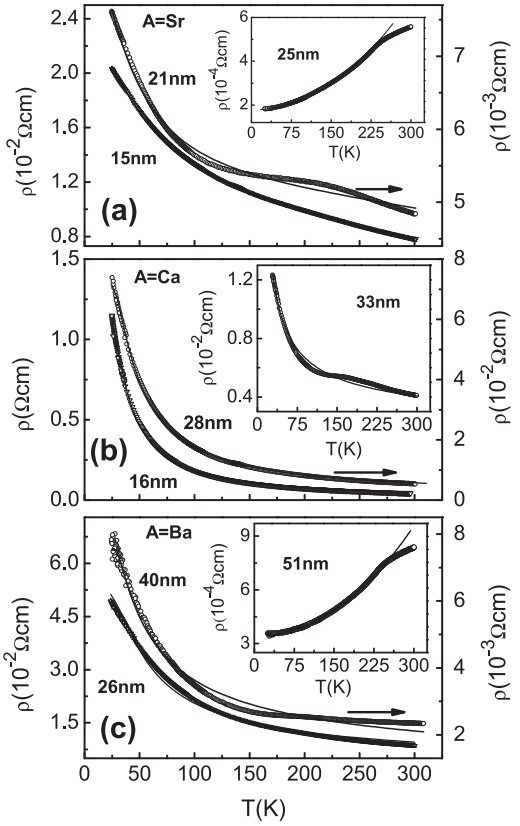

Fig. 3. Temperature dependence of resistivity of $La_{0.5}A_{0.5}CoO_3$ nanoparticles where (a) A = Sr, (b) A = Ca and (c) A = Ba. The solid lines in the inset of (a) and (c) present the best fit with Eq. (3) in the metallic region of 25 nm and 51 nm samples. In the insulating samples the solid lines represent the theoretical curves obtained by fitting with Eq. (2).

increase with the field and there is significant increase of MR with decreasing temperature and size of the samples.

3.4. Magnetic properties

3.4.1. dc magnetization

Fig. 5(a) and (c) presents the ZFC and FC $M(T)$ curves for $La_{0.5}Sr_{0.5}CoO_3$ and $La_{0.5}Ba_{0.5}CoO_3$, respectively whereas Fig. 5(b) presents the corresponding figures for $La_{0.5}Ca_{0.5}CoO_3$. The ZFC and FC magnetization show a large thermomagnetic irreversibility with irreversibility temperature (T_{irr}) close to T_C. T_C was determined by the minimum of the dM/dT versus T curves (Table 2). The width of transition δT_C, increases with the decrease of particle size. This broad transition suggests a possible existence of wide distribution of exchange interactions in the vicinity of the grain boundaries. The maximum in the $M_{ZFC}(T)$ curve is observed at a temperature (T_a) lower than (T_{irr}). Hysteresis measurements for Sr-doped and Ba-doped samples with 25 nm and 40 nm sizes are shown in Fig. 6(a) and (b), respectively. They show ferromagnetic behaviour with clear hysteresis. For Ba-doped sample coercive field (H_C) is 1562 Oe at 25 K whereas H_C = 400 Oe at 5 K for Sr-doped sample. Inset of Fig. 6(a) shows the magnetization versus magnetic field at temperature 5 K for the 25 nm sample.

3.4.2. ac magnetization

In Fig. 7 the *ac* susceptibility is plotted as a function of temperature for the 21 nm ((a) and (b)) and 15 nm ((c) and (d)) samples of $La_{0.5}Sr_{0.5}CoO_3$ and 16 nm ((e) and (f)) samples of $La_{0.5}Ca_{0.5}CoO_3$. Fig. 7(a), (c) and (e) presents the in-phase component ($\chi'(T)$) and (b), (d) and (f) show the out of phase component (χ'') of the *ac* susceptibility. In Fig. 7(a), (c) and (e), the high temperature maximum is found to be frequency independent and it shifts to low temperature with a decrease in size. The shoulder at T_f shifts to low temperature and finally disappears as size decreases. From Fig. 7(b) and (d) it is also observed that the high temperature peak position in the out of phase component of *ac* susceptibility $\chi''(T)$ shifts to low temperature with decrease in particle size. For the 21 nm samples, the high-temperature peak in $\chi''(T)$ appears at the same temperature as that in $\chi'(T)$ curve but they have different origins. The high-temperature peak in $\chi''(T)$ is related to the irreversibility temperature in dc $M(T)$. It should be noted that the shoulder in the $\chi'(T)$ curves and a peak in $\chi''(T)$ appeared at almost the same temperature (T_f). The temperature (T_f) increases with increase of excitation frequency. The low temperature peak may be attributed to the freezing of the ferromagnetic clusters. The peak clearly shifts to low temperature and the intensity of the peak is greatly reduced with the decrease in particle size.

4. Discussions

4.1. Resistivity

According to Golovanov et al. [16] in the parent compound $LaCoO_3$ the low spin Co^{3+} ions are thermally excited to high spin or intermediate spin states. The concentration of these excited Co atoms may be written as

$$n' = \frac{\nu}{\nu + \exp(\Delta/k_B T)} \tag{1}$$

where ν = 15 is the multiplicity of the high spin state and Δ is the spin gap. According to Señarís-Rodríguez [17] and Itoh et al. [6], hole-rich ferromagnetic clusters coexist with the hole-poor antiferromagnetic matrix in the cobaltites. The resistivity results can be explained by considering the nanoparticle system as a phase-separated compound consisting of FM clusters with Co^{4+} in an insulating matrix of Co^{3+} ions. Therefore $La_{0.5}A_{0.5}CoO_3$ nanoparticles can be considered as a random resistor network with percolating ferromagnetic clusters. For manganites two parallel-resistor model has been successfully applied to fit the temperature dependence of resistivity [18]. Considering metallic behaviour of FM clusters Prokhorov et al. [19] presented a modified empirical relation as

$$\frac{1}{\rho(T)} = \frac{n'\eta}{\rho_0 + \alpha T^2} + \frac{1-\eta}{\rho_\infty \exp[(T_0/T)^{1/4}]} \tag{2}$$

where n' is the population of excited Co^{3+} state described in Eq. (1). η is the FM phase fraction, which is assumed to be equal to divalent ion doping concentration. The first term describes the $\rho(T)$ behaviour of the FM phase where the charge exchange takes place between Co^{3+} and Co^{4+} via the double exchange mechanism in the ferromagnetic clusters and the second one comes, from the semiconductive or insulating matrix or grain boundaries. It is noteworthy that at high temperature since the resistance of the insulating channel is smaller than that of the ferromagnetic clusters, the conduction predominantly takes place through the insulator network. Again at low temperature the resistance of the insulating matrix is very much higher than that of the ferromagnetic region and the FM channel acts as the conductive path. The resistivity of the semiconducting samples fits well with the above parallel resistor model. In case of the resistivity of 21 nm Sr-doped, 33 nm Ca-doped and 40 nm Ba-doped samples the model cannot describe the $\rho(T)$ behaviour over the entire temperature range studied. The resistivity fits in the high and low temperature end but does not fit in the middle region where $\rho(T)$ is wavy shaped in nature.

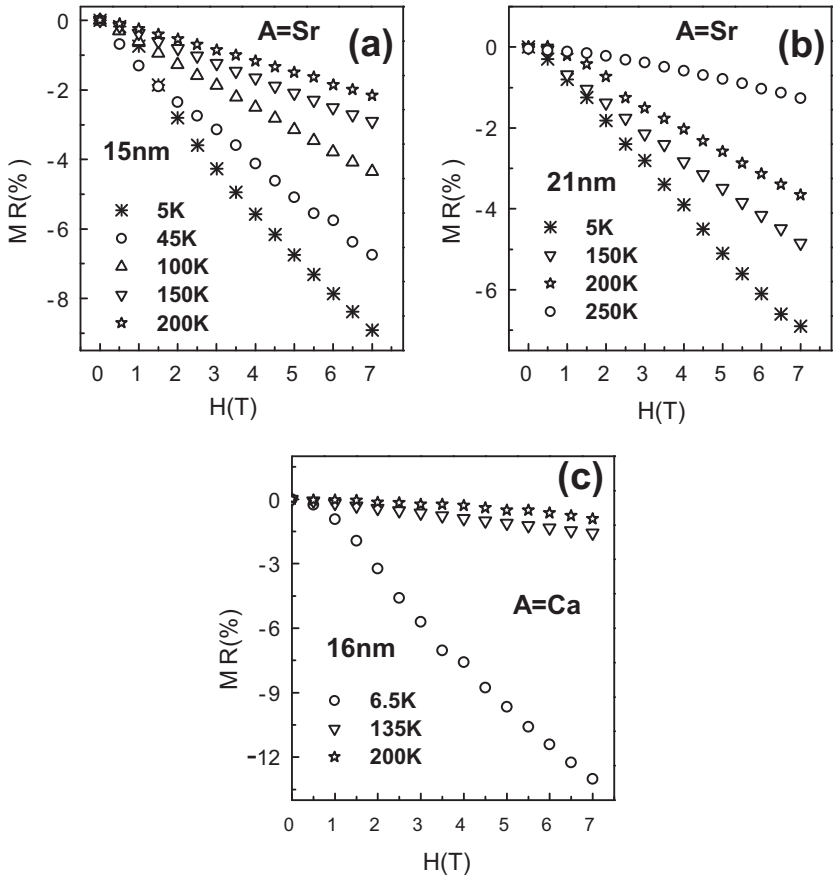

Fig. 4. Magnetic field variation of magnetoresistance of $La_{0.5}Sr_{0.5}CoO_3$ with size (a) 15 nm and (b) 21 nm and (c) $La_{0.5}Ca_{0.5}CoO_3$ with size 16 nm at different temperatures.

Below T_C, $\rho(T)$ fits well with the equation [20]

$$\rho(T) = \rho_0 + \rho_2 T^2 + \rho_{9/2} T^{9/2} \quad (3)$$

We have fitted the resistivity of the samples with the two parallel resistors model but from the figures (Fig. 3) it is evident that this model does not give a good fit to the experimental data for the samples with higher sizes but fits well with the resistivity data of the samples with lower sizes.

4.2. Magnetoresistance

From Fig. 4(a) and (b) it is found that the MR at the lowest temperature is almost linear and this type of dependence of MR on applied field arises when the spontaneous magnetization gradually increases with the field. Highest MR is obtained for the specimen with the small size. Disorder due to the nanosize may have an important role in creating the enhancement of the MR with decreasing size. The MR increases with increasing H as the local spin tends to align with the applied field and the spin scattering of the conduction electron reduces. The MR seems to originate from the field-induced stabilization of the FM order and the magnetic field suppresses critical FM fluctuations, thus facilitating the charge motion. MR is almost linear on field (H) and decreases without any sign of saturation up to the highest measuring field. The slope with field varies as the temperature is changed. In case of oxide perovskites, for example manganites, the MR scales with the sample magnetization, meaning that the resistivity decreases quickly with applied field for $T < T_C$, where M increases rapidly with H. Low temperature MR shows a significant difference between low field and high field regimes. Low field response occurs at $H < 5$ kOe and it is characterized by a sudden decrease in resistivity. But here MR(H) of $La_{0.5}Ca_{0.5}CoO_3$ nanoparticles with average 16 nm size shows (Fig. 4(c)) nearly linear behaviour without showing any demarcation of low field and high field regimes. Surface contribution is greater when the grain size is reduced. This may have a role in determining the characteristic behaviour of MR(H) of this Ca-doped cobaltate.

4.3. Magnetic properties

4.3.1. dc magnetization

The large difference between the FC and ZFC magnetization indicates that the samples have short-range ferromagnetic interactions. It should be noted that the cusp in the ZFC magnetization

Table 2
Various characteristic temperatures and effective magnetic moment obtained from the analysis of the magnetic data.

Compounds	Sample (nm)	T_C (K)	δT_C (K)	T_a (K)	T_{irr} (K)	Θ (K)	μ_{eff} (μ_B)
$La_{0.5}Sr_{0.5}CoO_3$	15	190	30	165	189	215	2.37
	21	225	23	204	218	239	2.59
	25	242	10	207	230	247	3.81
$La_{0.5}Ca_{0.5}CoO_3$	16	175	15	170	187	182	1.65
$La_{0.5}Ba_{0.5}CoO_3$	40	180	4	140	190	200	3.49

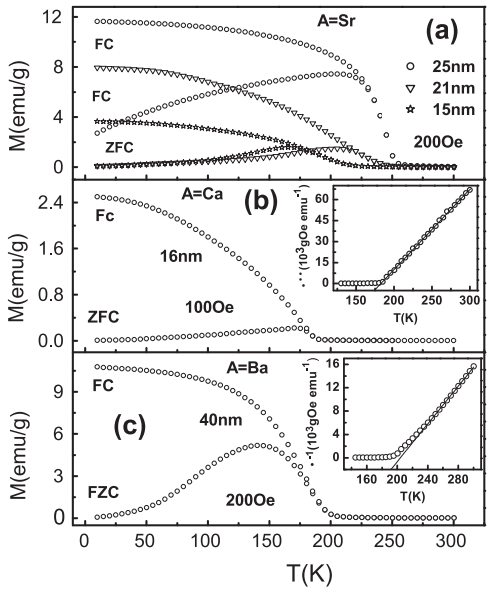

Fig. 5. Plot of dc magnetization versus temperature for (a) $La_{0.5}Sr_{0.5}CoO_3$, (c) $La_{0.5}Ba_{0.5}CoO_3$ samples, recorded at 200 Oe and (b) $La_{0.5}Ca_{0.5}CoO_3$ at 100 Oe under FC and ZFC conditions. The inverse of the dc susceptibility against temperature for $La_{0.5}Ca_{0.5}CoO_3$ and $La_{0.5}Sr_{0.5}CoO_3$ samples are shown in the inset and solid lines represent the fit to the Curie–Weiss law.

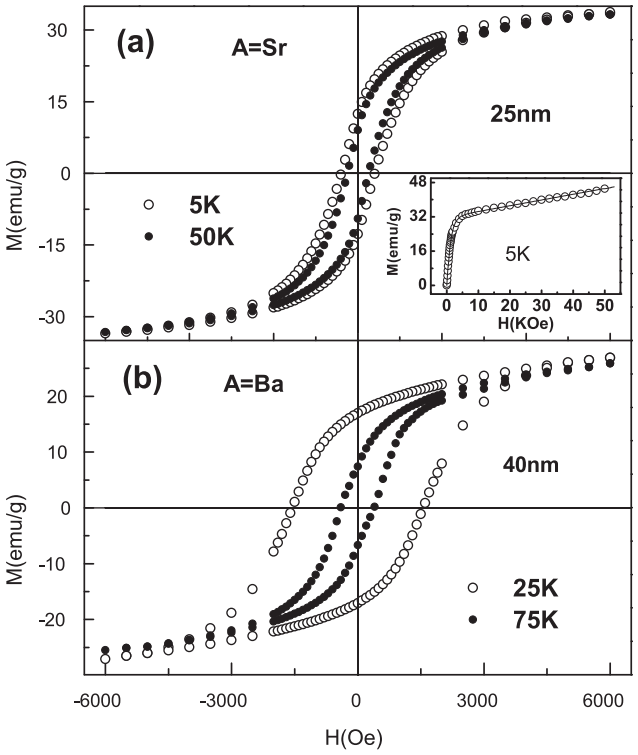

Fig. 6. Magnetization of (a) $La_{0.5}Sr_{0.5}CoO_3$ with 25 nm and (b) $La_{0.5}Ba_{0.5}CoO_3$ with 40 nm size plotted as a function of H for different temperatures. Inset in (a) shows the magnetic field variation of magnetization of the 25 nm sample of $La_{0.5}Sr_{0.5}CoO_3$ at 5 K along with the fitted curve.

appears for all the samples and this is one of the characteristic features of spin glass, cluster glass, re-entrant spin glass, superparamagnet, etc. [6,21]. For spin glass systems, the spin glass transition determines the nature of the $M_{ZFC}(T)$ cusp which appears where spin glass freezes. But for cluster glass, the $M_{ZFC}(T)$ cusp is governed by the anisotropy field acting on the spins inside each cluster. The appearance of the peak in the ZFC magnetization can be interpreted in terms of a competition between the local anisotropy field originating from individual FM clusters and the applied magnetic field. The magnetic moments of the spins in the ferromagnetic clusters freezes in the directions which are energetically favoured by the anisotropy field or the applied magnetic field during cooling. The anisotropy field plays the dominant role in temperature region $T < T_a$ but the applied field is predominant in the temperature regime $T > T_a$. The average anisotropy energy may be written as $E_a(T) = H_a(T) \times M(T)$ and the energy due to the applied field is $E_{ex}(T) = H_{ex} \times M(T)$. Here $H_a(T)$ and $M(T)$ are the temperature dependences of the average anisotropy field and magnetization, respectively and H_{ex} is the external field. The broad cusp at T_a marks a crossover region where $E_a(T)$ and $E_{ex}(T)$ are comparable. In the paramagnetic regime, the samples obey the Curie–Weiss (CW) law (inset of Fig. 5(b) and (c)). The paramagnetic Curie temperature (Θ) steadily decreases with decrease of the size (Table 2). To elucidate the spin states of the cobalt ions in the various samples, the effective magnetic moment μ_{eff} is calculated from the linear part of the Curie–Weiss regime. The value of the effective magnetic moment μ_{eff} decreases with decreasing size. In the $La_{0.5}Sr_{0.5}CoO_3$ system, the total spin can be expressed as $S_{spin} = 0.5S_3 + 0.5S_4$, where S_3 and S_4 represent the spin of Co^{3+} and Co^{4+} ions, respectively. From the theoretical and experimental studies [5,22–27] it is now established that the Co^{3+} ions exists in the IS state in $La_{1-x}A_xCoO_3$ compounds, but the spin state of Co^{4+} ions is still an open issue. The Co^{4+} ions can exist in the LS state, IS state, HS state or a mixture of these states [8]. If we assume that in the 25 nm sample of $La_{0.5}Sr_{0.5}CoO_3$ Co^{3+} ions are in the IS($S_3 = 1$) state but the Co^{4+} ions are in both the IS($S_4 = 1.5$) and HS($S_4 = 2.5$) states in the ratio of 1:1 [28], the effective magnetic moment can be calculated according to the formula $\mu_{eff} = g[J(J+1)]^{1/2}\mu_B$, and considering the spin only value (i.e., $J = S_{spin}$), we get $\mu_{eff} = 3.87\mu_B$. In consistence with the previous reports [6,28,29] the spin distribution in the higher dimensional sample shows a good agreement between experimental and theoretical results. According to the anisotropy field model which is used to explain the peak of the ZFC curve, the $M(H)$ curve should not saturate at moderate magnetic field due to the existence of finite number of Co spins in nonmagnetic AF matrix. $M(H)$ curve of the 25 nm Sr-doped sample does not saturate up to 5 T field. In order to estimate the spin state of this sample we have followed the procedure proposed by Yamaguchi et al. [30]. The $M(H)$ data were fitted with the low of saturation of magnetization. The best fit is obtained for $J = 1.55$. It suggests that a mixture of spin configuration exists in 25 nm sample. The decrease of magnetization with the reduction of particle size as shown in Fig. 5(a) appears due to the enhancement of surface disorder with the decrease in particle size. In that case the above explanation should also consider the surface-core model of nanoparticles. In case of 40 nm sample of $La_{0.5}Ba_{0.5}CoO_3$ if we assume that Co^{3+} ions are in the IS state but the Co^{4+} are in the IS state and HS state in the ratio 0.9:0.1 then $S = 1.3$ so that the effective moment becomes $\mu_{eff} = 3.46\mu_B$. The experimental effective moment $3.49\mu_B$ agrees well with the calculated one. Therefore it is reasonable to believe that Co^{3+} resides in intermediate state and Co^{4+} ions stay in both IS and HS states.

4.3.2. ac magnetization

In the absence of any clear frequency dependence in its χ'' versus T curve, the analysis is performed on the basis of $\chi'(T)$ data. Each frequency corresponds to an observation time ($t_{obs} = 1/f$) characteristics of the measurement. One can define from each susceptibility curve a frequency dependent freezing temperature (T_f), below which the longest relaxation time of the system exceeds t_{obs}, and the system is out of equilibrium. The peak at T_f shifts towards higher temperatures with higher frequencies. The tem-

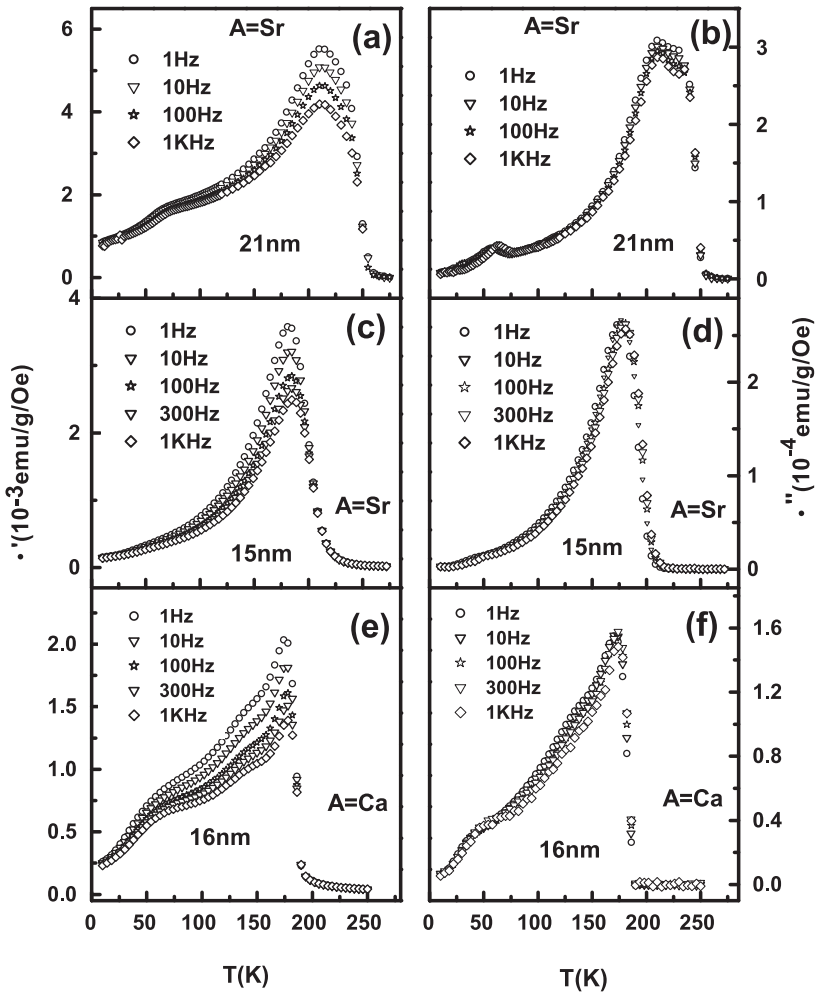

Fig. 7. Plots of real part ((a), (c) and (e)) and imaginary part ((b), (d) and (f)) of *ac* magnetization versus temperature at different frequencies for the $La_{0.5}Sr_{0.5}CoO_3$ and $La_{0.5}Ca_{0.5}CoO_3$ compounds.

perature shift per decade defined as $(\Delta T_f/(T_f \Delta \log f))$ was calculated to be 0.038–0.046 assuming T_f is the peak temperature of χ'. The value is comparable to those reported for cluster glasses [31]. This result shows the existence of a weakly frustrated state, such as cluster glass, originated from coexisting antiferromagnetic interactions between Co ions and surface disorder. We have estimated the freezing temperature (T_g) by extrapolating the T_f versus frequency curve to zero frequency. The frequency dependence can be well described invoking the critical slowing down of the spin dynamics [8,32] expressed as $\tau/\tau_0 = [(T_f - T_g)/T_g]^{-z\nu}$ where τ is the relaxation time $\propto f^{-1}$, τ_0 is the characteristic time constant and $z\nu$ is a critical exponent. The best fit to $\log(\tau)$ versus $\log[(T_f - T_g)/T_g]$ curve is shown in Fig. 8(a) and (b), and a good scaling is obtained for $\tau_0 = 5.14 \times 10^{-9}$ s, 1.19×10^{-8} s, and $T_g = 45$ K, 53 K, $\nu z = 7.46$, 9.59 for the 21 nm Sr-doped sample and 16 nm Ca-doped sample, respectively. Therefore the analysis of the *ac* susceptibility data reveals the cluster glass nature of $La_{0.5}A_{0.5}CoO_3$ nanoparticles, originated from co-existing antiferromagnetic interactions between Co ions and surface disorder.

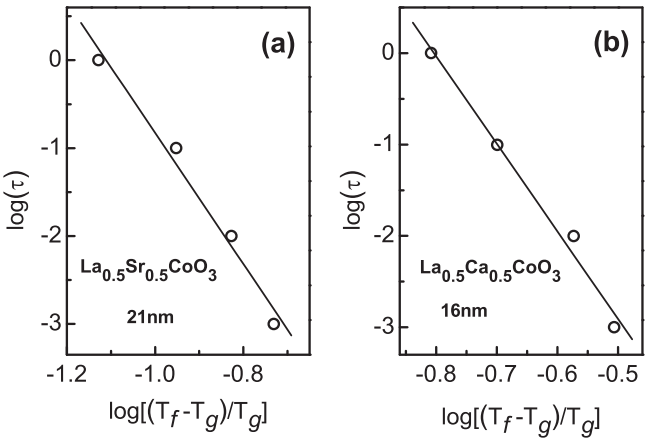

Fig. 8. The $\log(\tau)$ versus $\log[(T_f - T_g)/T_g]$ of the (a) 21 nm $La_{0.5}Sr_{0.5}CoO_3$ and (b) 16 nm $La_{0.5}Ca_{0.5}CoO_3$ samples.

5. Conclusion

In summary, we have investigated the size-induced metal to insulator transition and glassy magnetic behaviour in $La_{0.5}A_{0.5}CoO_3$ (A = Sr, Ca, and Ba) nanoparticles. The resistivity behaviour displays a size-induced metal to insulator transition. The field variation of magnetoresistance highlights the rapid evolution of magnetotransport properties. MR(H) shows an almost linear behaviour throughout the field range studied. The magnetization values suggest that Co^{3+} ions are in the IS state, while Co^{4+} ions suggest that Co^{3+} ions are in the IS state, while Co^{4+} ions are in a mixture of its IS and HS states. The magnetization decreases due to the enhancement in the surface disorder with the decrease in particle size. In the

ac susceptibility measurements, the shift of the low temperature peak in $\chi'(T)$ and $\chi''(T)$, which corresponds to the freezing of the ferromagnetic clusters, indicates that the size of the cluster decreases with decrease of particle size. The frequency shift per decade is found to be 0.038–0.046 which indicates that the samples fall in the cluster glass category. The static and dynamic magnetic behaviour uphold a cluster glass-like state of the nanoparticles. Except for the absence of metallic character in $La_{0.5}Ca_{0.5}CoO_3$ nanoparticles, the properties of Ca and Ba doped cobaltates have close resemblance with those of $La_{0.5}Sr_{0.5}CoO_3$ nanoparticles. Though glassy properties are also exhibited by the bulk samples, this character is very much pronounced in the nanoparticles due to the enhancement of the surface disorder.

Acknowledgements

We thank Mr. A.K. Pal for technical assistance and Mr. Pulak Roy of Biophysics division of SINP for providing us the TEM facility.

References

[1] P.M. Raccah, J.B. Goodenough, J. Phys. Rev. 155 (1967) 932.
[2] V.G. Bhide, D.S. Rajoria, Y.S. Reddy, G.R. Rao, G.V. Subba Rao, C.N.R. Rao, Phys. Rev. Lett. 28 (1972) 1133.
[3] V.G. Bhide, D.S. Rajoria, G.R. Rao, C.N.R. Rao, Phys. Rev. 6 (1972) 1021.
[4] K. Asai, P. Gehring, H. Chou, G. Shirane, Phys. Rev. B 40 (1989) 10982.
[5] M.A. Korotin, S.Yu. Ezhov, I.V. Solovyev, V.I. Anisimov, D.I. Khomskii, G.A. Sawatzky, Phys. Rev. B 54 (1996) 5309.
[6] M. Itoh, I. Natori, S. Kubota, K. Motoya, J. Phys. Soc. Jpn. 63 (1994) 1486.
[7] K. Asai, O. Yokokura, N. Nishimori, H. Chou, J.M. Tranquada, G. Shirane, S. Higuchi, Y. Okajima, K. Kohn, Phys. Rev. B 50 (1994) 3025.
[8] J. Wu, C. Leighton, Phys. Rev. B 67 (2003) 174408.
[9] R. Kreiner, C. Zobel, A. Reichl, J. Baier, M. Cwik, K. Berggold, H. Kierspel, O. Zabara, A. Freimuth, T. Lorenz, Phys. Rev. B 69 (2004) 094417.
[10] R. Ganguly, A. Maignan, C. Martin, M. Hervieu, B. Raveau, J. Phys.: Condens. Matter 14 (2002) 8595.
[11] Ch. Zock, L. Haupt, K. Baerner, B.M. Todris, K. Asadov, E.A. Zavadskii, T. Gron, J. Magn. Magn. Mater. 150 (1995) 253.
[12] J. Rodriguez-Carvajal, Physica B 192 (1993) 55.
[13] Y.M. Xiong, Y.R. Lu, X.G. Luo, Y. Zhang, P.H. Li, L. Huang, X.H. Chen, J. Magn. Magn. Mater. 299 (2006) 188.
[14] K. Yoshi, A. Nakamura, Mater. Res. Bull. 36 (2001) 144.
[15] B. Roy, S. Das, Appl. Phys. Lett. 92 (2008) 233101.
[16] V. Golovanov, L. Mihaly, A.R. Moodenbaugh, Phys. Rev. B 53 (1996) 8207.
[17] M.A. Señarís-Rodríguez, J.B. Goodenough, J. Solid State Chem. 118 (1995) 323; M.A. Señarís-Rodríguez, J.B. Goodenough, J. Solid State Chem. 116 (2004) 224.
[18] C. Zener, Phys. Rev. 82 (1951) 403.
[19] G. Prokhorov, G.G. Kaminsky, I.I. Kravchenko, Y.P. Lee, Physica B 324 (2002) 205.
[20] B. Roy, A. Poddar, S. Das, J. Appl. Phys. 100 (2006) 104318.
[21] D.N.H. Nam, K. Jonason, P. Nordblad, N.V. Khiem, N.X. Phuc, Phys. Rev. B 59 (1999) 4189.
[22] R.H. Potze, G.A. Sawatzky, M. Abbate, Phys. Rev. B 51 (1995) 11501.
[23] M. Magnuson, S.M. Butorin, C. Sathe, J. Nordgren, P. Ravindran, Europhys. Lett. 68 (2004) 289.
[24] T. Saitoh, T. Mizokawa, A. Fujimori, M. Abbate, Y. Takeda, M. Takano, Phys. Rev. B 55 (1997) 4257.
[25] Y. Kobayashi, N. Fujiwara, S. Murata, K. Asai, H. Yasuoka, Phys. Rev. B 62 (2000) 410.
[26] C. Zobel, M. Kriener, D. Bruns, J. Baier, M. Grűninger, T. Lorenz, Phys. Rev. B 66 (2002), 020402(R).
[27] K. Asai, A. Yoneda, O. Yokokura, J.M. Tanquada, G. Shirane, K. Kohn, J. Phys. Soc. Jpn. 67 (1998) 290.
[28] X. Xu, L. Jiang, J. Shen, Z. Chen, Z. Xu, Phys. Lett. A 351 (2006) 431.
[29] K. Yoshii, H. Abe, Phys. Rev. B 67 (2003) 094408.
[30] S. Yamaguchi, Y. Okimoto, H. Taniguchi, Y. Tokura, Phys. Rev. B 53 (1996) R2926.
[31] J.A. Mydosh, Spin Glasses: An Experimental Introduction, Taylor & Francis, London, 1993.
[32] K. Gunarsson, P. Svedlindh, P. Nordblad, L. Lundgren, Phys. Rev. B 61 (1988) 754.